

PACS numbers: 52.50.Jm; 52.35.Tc
DOI: 10.1070/QE2008v038n01ABEH013601

Gas-dynamic effects in the interaction of a motionless optical pulsating discharge with gas

V.N. Tishchenko, G.N. Grachev, A.A. Pavlov, A.L. Smirnov, Al.A. Pavlov, M.P. Golubev

***Abstract*. The effect of energy removal from the combustion zone of a motionless optical pulsating discharge in the horizontal direction along the axis of a repetitively pulsed laser beam producing the discharge is discovered. The directivity diagram of a hot gas flow is formed during the action of hundreds of pulses. The effect is observed for short pulse durations, when the discharge efficiently generates shock waves. For long pulse durations, the heated gas propagates upward, as in a thermal source.**

Keywords: *repetitively pulsed laser radiation, optical pulsating discharge, shock waves.*

The stability of an optical discharge produced by cw laser radiation depends on the energy balance between the absorbed radiation and removed heat [1]. These processes are also important [2] for an optical pulsating discharge (OPD) initiated by focused repetitively pulsed radiation with a pulse repetition rate f of tens of kilohertz. To obtain the high absorption ($\sim 70\,\%$) of repetitively pulsed radiation in an OPD, it is necessary to replace gas in the OPD combustion zone, for example, by moving rapidly the focus [3] or producing the OPD in a gas flow or a narrow jet [4, 5]. In this case, the motion velocity of the focal plane, where radiation is produced ('the OPD velocity'), the length of sparks, their energy and frequency f are interrelated, which restricts the range of admissible OPD parameters. It seems that this restriction will be eliminated by using the anomalous effect of the energy removal from the OPD combustion zone along the laser beam axis considered in this paper. Note that a stationary heat source in motionless gas produces the rising convective flow of heated gas.

In this paper, we study the influence of the laser radiation and medium parameters on the structure of the field of perturbations produced by a motionless OPD in the environment. We measured the formation time of quasi-stationary perturbation structures and controlled the stability of absorption of repetitively pulsed radiation by the emission of the OPD plasma. A new method of the shadow visualisation of weak inhomogeneities is described.

An OPD represents laser sparks repeating at a high frequency. The sparks create shock waves and caverns with a high temperature and a low density of a few percent of the unperturbed gas density. Pressure in a spark is equalised with the pressure of a surrounding gas for the time 5 – 10 μs, and density – for the time ~ 1 ms [6 – 8], which is much longer than the time interval $1/f$ between pulses. The absorption of several radiation pulses should be accompanied by the gas 'burning out' in the focal region, resulting in an increase in the optical breakdown threshold and a decrease in the UV radiation intensity and a decrease in radiation absorption. The latter can be manifested in the fact that not each of the pulses will produce a spark.

The effect discovered in our paper is unusual for the following reason. The system under study has two selected directions: the gravity force direction and the laser beam axis. The heated gas, as in a thermal source, should be carried by a convective flow upward. According to the adopted concepts, the laser beam orientation should not affect the heat-and-mass transfer because radiation is absorbed over the spark length ~ 0.5 cm, which is comparable with its dynamic radius R_d, which is much smaller (approximately by 20 times) than the length of the observed horizontal heated gas flow (~ 10 cm).

The scheme of the experiment is shown in Fig. 1. The output power of a repetitively pulse CO_2 laser is insufficient for the optical breakdown of air. Because of this, an OPD was initiated in a chamber of volume 60 L filled with inert gases (argon or an argon – helium mixture), which have a lower breakdown threshold than air. The laser pulse duration was ~ 1 μs, and the duration of the first peak was ~ 0.3 μs. In some cases, periodic pulse trains or ~ 3-μs pulses were used. The pulse repetition rate was $f = 6 - 25$ kHz. For high f, the pulse energy was lower than the OPD burning threshold. The laser beam diameter on a focusing lens with the focal distance 17 cm was ~ 3 cm. The stability of absorption of laser pulses was controlled by a photodetector detecting the emission of laser sparks. The diameter of the region of optical diagnostics was 10 cm.

We present in the paper the fragments of photographs demonstrating perturbations of the medium. The chamber walls did not affect the results of measurements (see below). To record the maximum length of the perturbed region, the focus and the OPD burning in it are displaced to the edge of

V.N. Tishchenko, G.N. Grachev, A.L. Smirnov Institute of Laser Physics, Siberian Branch, Russian Academy of Sciences, prosp. akad. Lavrent'eva 13/3, 630090 Novosibirsk, Russia; e-mail: tishenko@mail.nsk.ru, grachev@laser.nsc.ru
A.A. Pavlov, Al.A. Pavlov, M.P. Golubev S.A. Khristanovich Institute of Theoretical and Applied Mechanics, Siberian Branch, Russian Academy of Sciences, ul. Institutskaya 4/1, 630090 Novosibirsk, Russia; e-mail: pavalex@itam.nsc.ru

Received 15 April 2007
Kvantovaya Elektronika **38** (1) 82 – 87 (2008)
Translated by M.N. Sapozhnikov

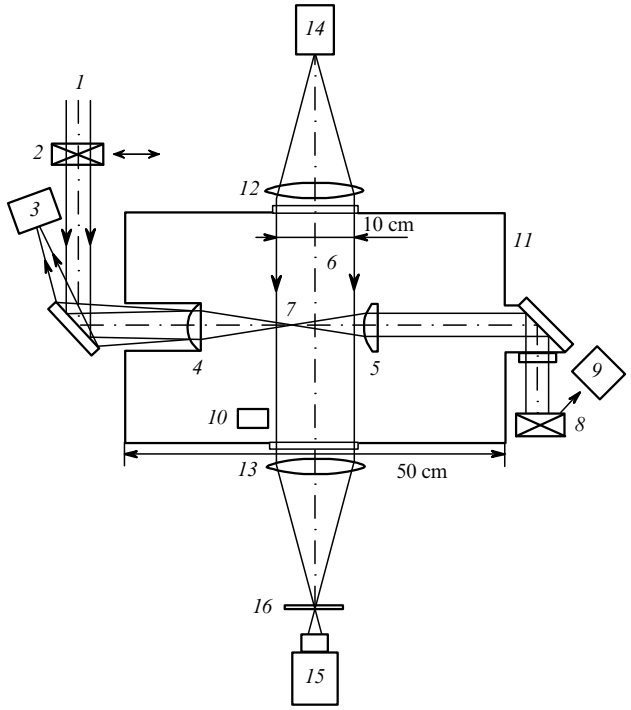

Figure 1. Scheme of the experimental setup: (*1*) repetitively pulsed laser beam; (*2*, *8*) TI-4 power meters; (*3*, *9*) FD511-2 laser pulse shape detectors; (*4*, *5*) lenses with the focal distances 17 and 13 cm; (*6*) optical diagnostics region; (*7*) OPD; (*10*) laser spark emission detector; (*11*) chamber; (*12*, *13*) collimator lenses of the shadow visualisation system; (*14*) laser; (*15*) PCO.SensiCam TV camera; (*16*) visualising transparency.

the shadow diagnostics region (Fig. 2). The pulse energies q_{in} and q_{ab} and the average powers W_{in} and W_{ab} of the input and absorbed radiation, respectively, are given in captions to Figs 2–7. In Figs 2, 4–6 is indicated the delay time t_{del} of the recording instant with respect to the OPD ignition instant.

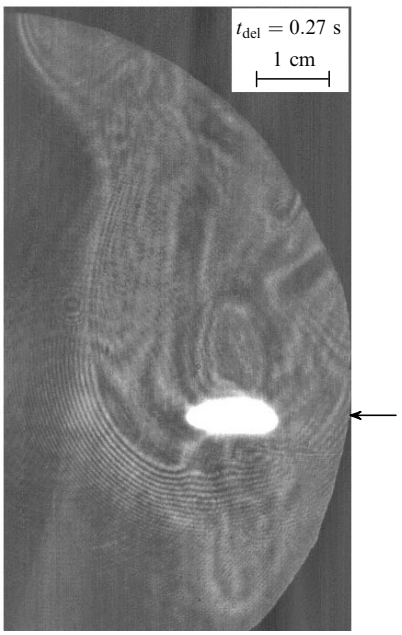

Figure 2. Convective flow produced by the OPD for the laser pulse duration ~ 30 μs, pulse repetition rate $f = 11$ kHz, average powers $W_{in} = 1.7$ kW and $W_{ab} = 0.45$ kW, and pulse energies $q_{in} = 0.155$ J and $q_{ab} = 0.041$ J. The arrow shows the laser beam direction.

The inhomogeneity of the gas density was visualised by shadow methods. The optical scheme presented in Fig. 1 contains collimator (*12*) and receiving (*13*) objectives, laser (*14*), and PCO.SensiCam TV camera (*15*) allowing the recording of a series of images synchronised from an external source. The exposure time could be varied from 500 ns to 10^3 s and the spatial resolution over the image field was 1280×1040 pixels.

At the first stage, a 'direct-shadow' scheme was used (without transparency visualisation). The sensitivity of this scheme depends on the degree of image defocusing. The second derivatives of the optical path (density) integral are recorded in the direction orthogonal to the radiation propagation direction. This scheme has an important disadvantage consisting in the geometrical distortion of the object under study, which increases with increasing sensitivity. Typical shadow images are presented in Fig. 3.

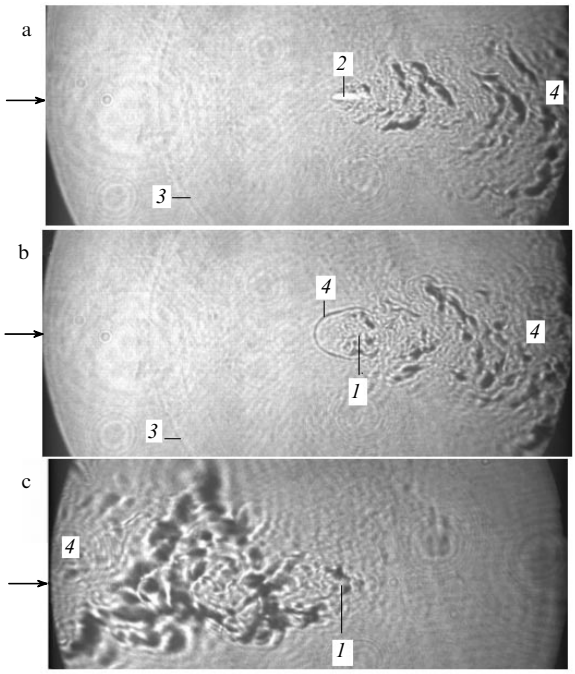

Figure 3. Shadow photographs of perturbations produced by the OPD in argon for $f = 12$ kHz, $W_{in} = 1.26$ kW, $q_{in} = 0.105$ J (the time interval between frames is 0.125 s) (a, b) and in the Ar : He = 0.7 : 0.3 atm mixture for $f = 25$ kHz, $W_{in} = 1.82$ kW and $q_{in} = 0.07$ J (c): (*1*) focal region; (*2*) spark; (*3*) shock-wave front; (*4*) heated gas flow from the OPD region; the horizontal size of the frame is 10 cm; the arrows show the laser beam direction.

To enhance the sensitivity and reduce geometrical distortions of the object, we used a shadow scheme with phototropic glass plate (*16*) (Fig. 1) as a visualising transparency [hereafter, the adaptive visualising transparency (AVT)]. It is known that the sensitivity of shadow methods using the Foucault knife is inversely proportional to the size of the light source image. The sensitivity can be increased by using coherent laser radiation with a small diffraction spot. However, in this case the undesirable noise due to diffraction from the knife edge is observed. In addition, the

influence of random displacements of optical elements and vibrations of the setup on the scheme alignment increases.

When an AVT is used, the action of a focused laser beam on the AVT causes the darkening of a region of size equal to the diffraction spot diameter. As a result, the sensitivity of the system considerably increases due to the obtainment of the minimal possible size of the light source image and the increase in the relative change in the image brightness in irradiated regions. Also, the influence of diffraction from the AVT decreases.

The absorption coefficient G of a thin AVT can be written in the form

$$G = \frac{I\theta_{ac}}{I\theta_{ac} + \theta_{dac}}\{1 - \exp[-(I\theta_{ac} + \theta_{dac})t]\}G_{max}, \quad (1)$$

where I is the incident radiation intensity; G_{max} is the maximal possible absorption coefficient; and t is time. The coefficients θ_{ac} and θ_{dac} depend on the properties of the AVT material and characterise the activation and deactivation rates of absorbing centres. The quantity $\tau_{ac} = 1/(I\theta_{ac})$ is the characteristic activation time and $\tau_{dac} = 1/\theta_{dac}$ is the deactivation time of absorbing centres. For the AVT material used here, $\tau_{dac} \sim 10^2$ s, while the activation time in the focal region of probe radiation (in the absence of perturbations) is $\tau_{ac} \sim 1$ s. Irradiation was performed by the 0.53-μm second harmonic line of a diode-pumped 54-mW neodymium laser.

The following limiting cases are important for an understanding of the AVT operation:

$$G \approx \frac{I\theta_{ac}}{I\theta_{ac} + \theta_{dac}}G_{max} \quad \text{for } t \gg 1/(I\theta_{ac} + \theta_{dac}), \quad (2)$$

$$G \approx G_{max} \quad \text{for } t \gg 1/(I\theta_{ac} + \theta_{dac}), I\theta_{ac} \gg \theta_{dac}, \quad (3)$$

$$G \approx \frac{I\theta_{ac}}{\theta_{dac}}G_{max} \quad \text{for } t \gg 1/(I\theta_{ac} + \theta_{dac}), I\theta_{ac} \ll \theta_{dac}, \quad (4)$$

$$G \approx I\theta_{ac}G_{max}t \quad \text{for } t \ll 1/(I\theta_{ac} + \theta_{dac}). \quad (5)$$

The blackening of the AVT in the focal region of radiation transmitted through the volume under study without distortions, where the greater part of energy falls, is described by relations (2) and (3). The corresponding regions of the image will be most darkened. The radiation experiencing small angular deviations even from a weak inhomogeneity propagates through a less darkened region of the AVT. In this case, the blackening is described by relation (4) for stationary inhomogeneities and by relation (5) for nonstationary inhomogeneities. These inhomogeneities are manifested as brighter regions on the image. The additional advantage of this method is that strong perturbations lead to the darkening of the corresponding sites of the AVT, so that the image clarification in the regions of large density gradients (for example, near shock-wave fronts) is considerably less pronounced than in the usual scheme, and does not suppress weaker perturbations existing against their background. The scheme is self-adjustable, which simplifies measurements. All the photographs, except in Fig. 3, were taken by using the AVT, which improved the sensitivity and quality of visualisation

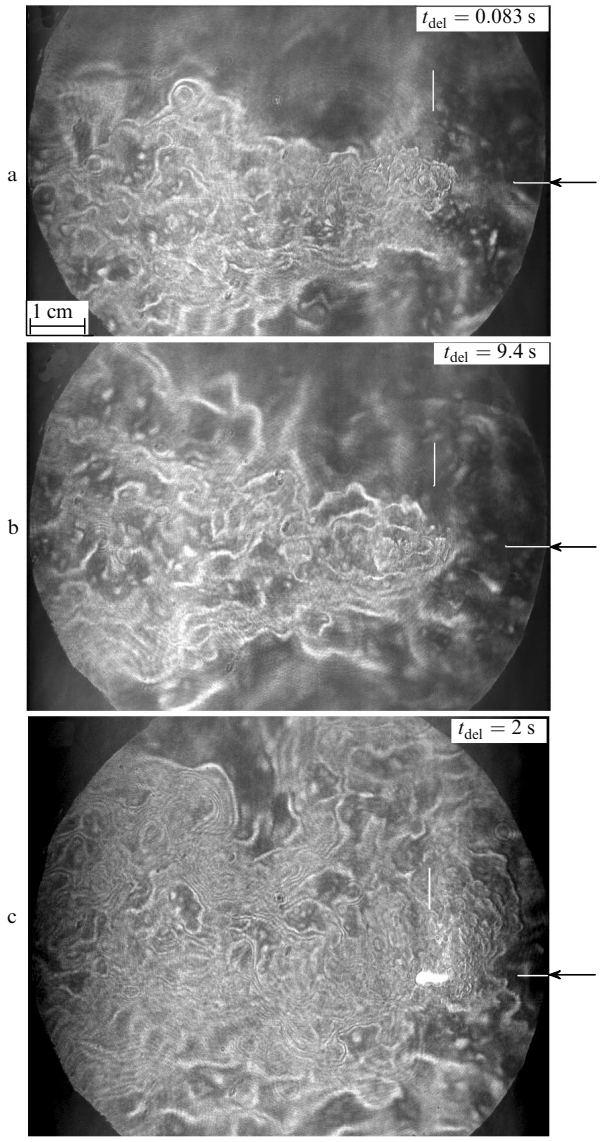

Figure 4. Typical perturbation patterns produced by repetitively pulsed radiation for $f = 12$ kHz, $W_{in} = 0.894$ kW, $W_{ab} = 0.256$ kW, $q_{in} = 0.0745$ J, and $q_{ab} = 0.0213$ J (a, b) and by trains of three pulses (separated by the time ~ 12 μs) with $F = 12$ kHz, $W_{in} = 1.29$ kW, $W_{ab} = 0.41$ kW, and the train energies $Q_{in} = 0.108$ J and $Q_{ab} = 0.034$ J (c). The arrows show the laser beam direction; the focus is located at the intersection of horizontal and vertical white bars. Photographs have the same scale.

of the density perturbation field (cf., for example, Figs 3 and 4).

Figure 2 presents the shadow photograph of perturbations produced by an OPD close to a continuous optical discharge. The duration of laser pulses was ~ 30 μs. The front peak produces a spark and a weak shock wave because the peak energy is small compared to the total pulse energy. Because the time of laser plasma expansion and pressure equalisation in a cavern and surrounding gas is ~ 5 μs (calculations), the absorption of the pulse tail is not accompanied by the formation of a shock wave. One can see from Fig. 2 that a rising gas flow is observed over the OPD region, as in a stationary thermal source. Due to the pulsed energy supply, the structure of perturbations is nonstationary both in the region of size of several milli-

metres and over the entire observation region (~ 5 cm). The region of perturbations preserves the upward elongated shape, while the shape of its boundary changes at the characteristic time scale less than 0.08 s (the time between video camera frames). The absence of shock waves is the main difference of this picture from the picture of perturbations upon OPD burning in the regime considered below, when the perturbation flow is directed horizontally along the beam axis.

Figure 3 presents, as Figs 4–7, the shadow photographs for the case of the OPD produced by ~ 1-μs pulses, which are shorter than the thermal expansion time of a spark. In this case, the OPD is a source of periodic shock waves. The directivity diagram of perturbations is oriented along the beam axis. A flow in the vertical direction is absent in the photograph. A video camera was switched on within ~ 1 s after the OPD ignition. The frame repetition rate was 12 Hz. Photographs demonstrate variations in a small-scale structure of perturbations and boundary shape from frame to frame, as well as small oscillations of the diagram axis with respect to the laser beam. Figure 3a demonstrates the spark emission. The photograph was taken within a short time after a successive optical breakdown. The spark emission is absent in Figs 3b, c. The photographs were taken with a large delay, and the plasma of a spark nearest in time cooled down to the temperature at which emission was not detected by the camera. Figure 3b demonstrates the instant of the departure of a shock-wave from the spark generating the wave. The same picture is observed in all photographs: shock waves are recorded in the unperturbed gas, while in the laser beam propagation direction a chaotic field of density pulsations is observed, from which shock waves are scattered. The pressure jump at the shock-wave front at a distance from the OPD region exceeding $10R_d \approx 5$ cm (where R_d is the dynamic radius of sparks) is small. The shock wave transforms to the acoustic perturbation. Hereafter, we will use the unified term – a shock wave.

The direction of the perturbation flow (along the laser beam or in the opposite direction) depends on the laser power. More exactly, it depends on the excess of the pulse energy over the optical breakdown threshold, which is determined by the gas type. This is illustrated in Fig. 3 for the maximum laser power and different mixtures and frequencies. In argon for $f = 12$ kHz, the pulse energy considerably exceeds the breakdown threshold, and, therefore, the perturbation field is oriented along the beam axis (Figs 3a, b). One can see from Fig. 3a that sparks are produced in a dense gas and efficiently transform laser radiation to shock waves. The readings of a pressure gauge show that each laser pulse generates a shock wave with the amplitude stable from pulse to pulse.

As the helium content in the Ar–He mixture was increased (at a total pressure of ~ 1 atm), the sound speed and optical breakdown threshold in gas increased. For the frequency $f = 12$ kHz, the direction of the perturbation flow in the Ar : He = 0.7 : 0.3 atm mixture, as in pure argon, coincides with the laser beam direction. In the same mixture, but for $f = 25$ kHz, as Fig. 3c shows, pulsations propagate in the opposite direction. The focus is located in the strongly perturbed gas. For some mixture compositions, the perturbation flow changes its direction during the OPD burning. The counterpropagating perturbation flow was also observed in experiments when the OPD was produced by low-power radiation.

The formation of horizontal perturbation flows and their typical structures are shown in Figs 4–6, which were obtained by a modified shadow method. The OPD was produced at a lower radiation power $W_{in} \approx 0.9$ kW (compared to W_{in} in Fig. 3). The pulse duration was ~ 1 μs. The OPD burning stability or its instability (some pulses or their trains did not produce sparks) was controlled by shadow photographs and by laser plasma emission detected with a photodiode. The video detection of the OPD was performed for ~ 10 s with a frame repetition rate of 12 Hz.

Typical perturbation patterns corresponding to the stable OPD burning and the horizontal orientation of the flow are shown in Figs 4a, b. Perturbations appeared over the entire length of the observation region already within ~ 0.083 s after the OPD ignition. No qualitative or quantitative difference between the first and last frames was observed. This suggests that the horizontal carrying out of perturbations is not related to the influence of chamber walls. At the same time, as for the regime corresponding to Figs 3a, b, the diagram shape and its small-scale structure changed from frame to frame. For low powers, unlike Fig. 3, the focus is located in the perturbed gas (Fig. 4). The position of sparks changes by less than ~ 1 mm during the OPD burning.

It is obvious that the removal of hot gas along the beam axis should be accompanied by the inflow of cold gas from the OPD surrounding. These are interrelated processes in which the hot gas removal is primary. The gas inflow is indirectly confirmed by the OPD burning stability, which is observed in oscillograms of the OPD plasma emission. Signal peaks in oscillograms correspond to individual laser pulses.

In the case of unstable OPD burning, the structure of the perturbation field is qualitatively different. Two typical pictures can be distinguished. The first picture is characterised by perturbations propagating oppositely to the laser beam propagation (Fig. 3c) or by the unstable (changing in time) orientation of the flow diagram. The second picture is characterised by the OPD burning regimes when perturbations fill the entire observation field, as shown in Fig. 4c, where the OPD was produced by laser pulse trains with a pulse repetition rate $F \approx 12$ kHz. Each of the trains contained three pulses separated by the time interval ~ 12 μs.

The formation dynamics of the directivity diagram of perturbations generated by the OPD is illustrated in Fig. 5. The photographs of perturbations taken at different times after the OPD ignition are presented. Each photograph corresponds to one OPD ignition. The camera was switched on with the delay t_{del} with respect to the first OPD spark because it was impossible to observe the dynamics after one ignition due to a low frame repetition rate: by the moment of the second frame exposure, the diagram of the perturbation flow has already formed. One can see from the photographs that after the OPD ignition the size of the perturbation zone increases with time. Its structure and shape are unstable and experience pulsations, and the selected direction is absent for $t < 25$ ms. The OPD is surrounded by a strongly inhomogeneous medium. Shock waves are observed at $t < 0.5$ ms, when the perturbation zone is small yet and shock waves are weakly scattered by them. Radiation produces ~ 300 sparks for the time $t \sim 25$ ms, the absorbed energy being ~ 5 J. The directivity diagram of the perturbation flow is formed by the moment $t \sim 50$ ms. For $t \sim 0.08$ s (~ 1000 pulses), the perturbation

flow overlaps the entire observation region (~ 10 cm, Fig. 4a). Thus, the characteristic transition time from chaotic pulsations of the gas density to their directional motion along the beam axis is 0.03 – 0.05 s, corresponding to the axial velocity $V \sim 0.1/0.05 = 2$ m s^{-1}. The removal of energy absorbed in the OPD at such small velocities V is possible only if the perturbed gas observed on photographs has a high temperature. Otherwise, the flow rate should be ~ 100 m s^{-1}. Note that the length of the perturbed region exceeded the distance between the OPD and lens (*5*) (Fig. 1), which resulted in the thermal damage of the lens within 20 – 30 min after the OPD ignition.

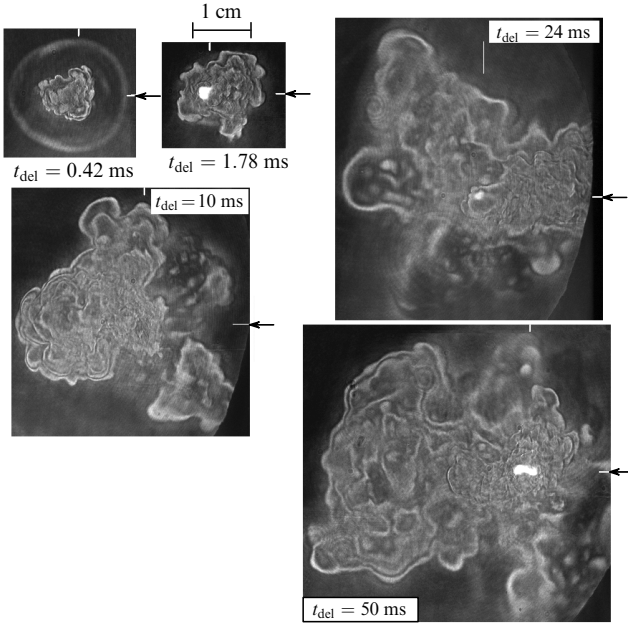

Figure 5. Shadow photographs of perturbations for $f = 12$ kHz, $W_{in} = 0.88$ kW, $W_{ab} = 0.23$ kW, $q_{in} = 0.073$ J, and $q_{ab} = 0.019$ J. The arrows show the laser beam direction; the focus is located at the intersection of horizontal and vertical white bars. Photographs have the same scale.

To understand the nature of the effect under study, it is important to known elementary perturbations generating the OPD. It is known that in the case of a single spark (Fig. 6a), a shock wave and a cavern are formed at the stage of adiabatic plasma expansion ($t < 10$ μs). The primary role of the shock wave was shown above: the hot gas of caverns is removed in the horizontal direction if shock waves are strong; otherwise, it is removed in the vertical direction. Elementary excitations also include a toroidal vortex (hereafter, a ring) produced by a single laser spark [9]. For $t > 30$ μs, a cold gas jet of length ~ 1 cm is formed on the spark axis, which propagates oppositely to the ~ 1-J laser radiation at a rate of ~ 150 m s^{-1} [9, 10]. In this case, the plasma is displaced to the periphery in the radial direction by forming an expanding vortex ring, which was observed for ~ 1 ms.

Typical elementary structures of the perturbation field produced by the motionless and moving OPDs are shown in Figs 6 and 7, respectively. When the motionless OPD is stable, density perturbations on photographs look chaotic (Fig. 4). For this reason, the search for structures was performed at a low excitation power, when the motionless OPD was unstable and quenched for the time 0.1 – 1 ms,

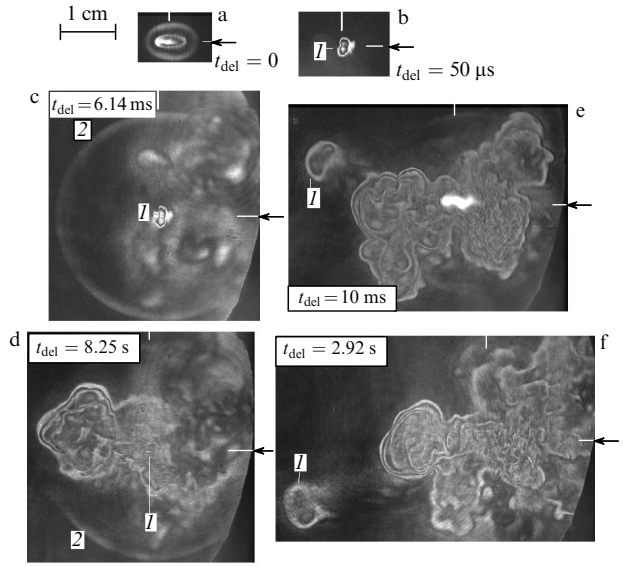

Figure 6. Typical perturbation patterns (*1* – ring, *2* – shock-wave front) produced by the motionless OPD from the first spark (a, b) and upon the repeated (spontaneous) ignition of the OPD, which was quenched before this for the time less than 0.1 s (c – f). The parameter of repetitively pulsed radiation were $f = 12$ kHz, $W_{in} = 0.57$ kW, and $q_{in} = 0.048$ J (a – d). The parameters of the trains of three pulses (separated by the time ~ 11 μs) were $F = 12$ kHz, $W_{in} = 1.29$ kW, $W_{ab} = 0.41$ kW, train energies $Q_{in} = 0.108$ J and $Q_{ab} = 0.034$J (e, f). The arrows show the laser beam direction; the focus is located at the intersection of horizontal and vertical white bars. Photographs have the same scale.

which is observed by the spark emission and shadow photographs. Photographs in Figs 6a, b correspond to perturbations caused by the first OPD spark. Figures 6c – f illustrate perturbations for the case when the OPD was ignited after a delay.

Figure 7 presents the shadow photographs of perturbations produced by moving OPDs. For the 'high OPD velocity', caverns are isolated from each other and do not affect each other (Figs 7a – c), while for small velocities they are partially overlapped (Fig. 7d). The cavern located

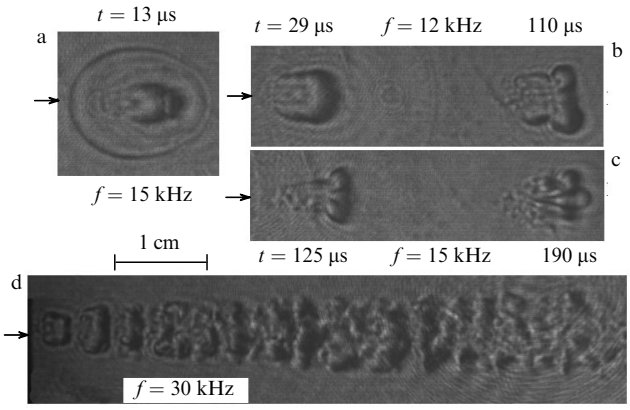

Figure 7. Shadow photographs of perturbations produced by the OPD (the focus of repetitively pulsed radiation was moved from left to right) moving at the velocity $v \sim 300$ m s^{-1} ($q_{ab} \sim 40 - 50$ mJ, $q_{in} = 2.5q_a$ (a-c) and $v \sim 100$ m s^{-1} ($q_{ab} \sim 24$ mJ, $q_{in} = 2.5q_{ab}$) (d); t is the spark lifetime. The arrows show the laser beam direction. Photographs have the same scale.

at the left of Figs 7a, b is the last one produced by radiation by the detection moment. The time indicated in Fig. 7 is measured from the instant of spark production. For example, the left cavern in Fig. 7b is the last one, and was produced by a spark 29 μs ago. The right cavern (produced by the previous spark) exists for ~ 110 μs. All the photographs in Figs 6 and 7 demonstrate the gas perturbation in the form of a ring. The initial existence stage of the rings is shown in Figs 6b–d. The ring in Fig. 6c formed due to the first breakdown after the short-time quenching of the OPD; also, perturbations produced before the OPD quenching are observed. Figure 6d shows the ring at the initial existence stage, which was formed within a long time after the repeated OPD ignition. Of most interest are rings located at a great distance from the OPD region (Figs 6e, f).

Neither shock waves nor vortex rings or a jet can explain, without the use of an additional mechanism, the large formation time (hundreds of pulses) of the perturbed gas flow and the fact itself of the gas flow propagation along the horizontal axis of radiation over a large distance, exceeding by a factor of 20 and more the spark length and its dynamic radius.

At the same time, the observed effect is not caused by the influence of the chamber walls – the pulling down of perturbations by reflected shock waves or the gas flow, which could appear due to gas heating in the chamber. This follows from quantitative estimates and the results of measurements presented below. The effect is observed after less than 0.1 s, when the energy absorbed in the OPD is insufficient yet for heating and acceleration of ~ 60 L of gas contained in the chamber. In addition, the structure of the perturbation flow after 0.1 and 10 s is the same (Figs 4a, b). In some experiments, we deliberately produced a gas flow with the help of a fan placed at the bottom of the chamber to mix argon and helium after their admission to the chamber. A weak influence of the fan was observed on the shadow photographs only in the regime of OPD formation by long pulses, when the hot gas flow was removed from the OPD region in the vertical direction. In this case, the upper part of the rising flow (at a distance of 3 cm from the OPD region) oscillates with respect to its axis and is more inhomogeneous than in Fig. 2, which was obtained when the fan was switched off.

By estimating the possible influence of the chamber and its elements on the effect under study, we should take into account the reflected shock waves and formation of the gas flow in the chamber. Shock waves reflected from a focusing lens could affect the formation of the hot gas flow from the OPD along the laser beam direction (Fig. 1). The propagation time of a shock wave from the OPD region to the lens and backward is $t_1 \sim 2L_1/c_0 \sim 1-3$ ms, which is much less than the formation time of the perturbation diagram $t_2 \sim 50$ ms. Here, $L_1 \approx 17$ cm is the distance from the OPD region to the lens and $c_0 = 320$ m s^{-1} is sound speed in argon. The reflected shock waves are not observed on shadow photographs because for $2L_1/R_d \sim 34/0.5 = 68$ they degenerate to weak acoustic oscillations. Note also that photographs in Fig. 3 were obtained by using the experimental scheme from paper [3], where lenses (*4*) and (*5*) were absent and a focusing system was located outside the chamber. The nearest reflecting surface was the chamber wall, which was located at a distance of 16 cm from the OPD region along the laser beam axis. One can see from Fig. 3 that this wall does not influence the effect under study. The time t_2 and energy (~ 10 J) absorbed for this time are too small to form the gas flow in the chamber.

Note that the OPD stability indicates that the cold gas entering the combustion zone compensates for the removal of the hot gas both in the vertical and horizontal directions.

Thus, in the case of short laser pulses, the energy absorbed in the OPD is removed by shock waves and the gas flow propagating in the laser beam direction. In the case of longer laser pulses, the gas is removed in the vertical direction by a convective flow, as in a thermal source. To develop a physical model of this effect, it is necessary to perform experiments with OPDs in air, which is possible by employing a 5-kW repetitively pulsed laser. The scaling methods for high-power lasers are developed in [11].

Acknowledgements. The authors thank A.G. Ponomarenko for the support of optical discharge investigations. This work was supported by the Russian Foundation for Basic Research (Grant No. 06-08-01192) and the Siberian Branch RAS (project No. 152).

References

1. Raizer Yu.P. *Lazernaya iskra i rasprostranenie razryadov* (Laser Spark and Discharge Propagation) (Moscow: Nauka, 1974).
2. Tishchenko V.N., Apollonov V.V., Grachev G.N., Gulidov A.I., Zapryagaev V.I., Men'shikov Ya.G., Smirnov A.L., Sobolev A.V. *Kvantovaya Elektron.*, **34**, 941 (2004) [*Quantum Electron.*, **34**, 941 (2004)].
3. Grachev G.N., Ponomarenko A.G., Smirnov A.L., Statsenko P.A., Tishchenko V.N., Trashkeev S.I. *Kvantovaya Elektron.*, **35**, 973 (2005) [*Quantum Electron.*, **35**, 973 (2005)].
4. Tret'yakov P.K., Grachev G.N., Ivanchenko A.I., Krainev V.L., Ponomarenko A.G., Tishchenko V.N. *Dokl. Ross. Akad. Nauk*, **336**, 466 (1994).
5. Borzov V.Yu., Mikhailov V.M., Rybka I.V., Savishchenko N.P., Yur'ev A.S. *Inzh.-Fiz. Zh.*, **66**, 515 (1994).
6. Kabanov S.N., Maslova L.I., Tarkhova T.I., Trukhin V.A., Yurov V.T. *Zh. Tekh. Fiz.*, **60**, 37 (1990).
7. Tishchenko V.N., Antonov V.M., Melekhov A.V., Nikitin S.A., Posukh V.G., Tret'yakov P.K., Shaikhislamov I.F. *Pis'ma Zh. Tekh. Fiz.*, **22**, 30 (1996).
8. Bel'kov E.P. *Zh. Tekh. Fiz.*, **44**, 1946 (1974).
9. Bufetov I.A., Prokhorov A.M., Fedotrov V.B., Fomin V.K. *Dokl. Akad. Nauk SSSR*, **261**, 586 (1981).
10. Kondrashev V.N., Rodionov N.B., Sitnikov S.F., Sokolov V.I. Preprint No. IAE-4154/7 (Moscow: I.V. Kurchatov Institute of Atomic Energy, 1985).
11. Apollonov V.V., Kiiko V.V., Kislov V.I., Suzdal'tsev A.G., Egorov A.B. *Kvantovaya Elektron.*, **33**, 753 (2003) [*Quantum Electron.*, **33**, 753 (2003)].